

The Structural Properties of Isolated Galaxies, Spiral-Spiral Pairs, and Mergers: The Robustness of Galaxy Morphology During Secular Evolution

H. M. Hernández-Toledo¹ and V. Avila-Reese²
Instituto de Astronomía, UNAM, A.P. 70-264, 04510 México D. F., México

C. J. Conselice³
California Institute of Technology, Pasadena, CA 91125, USA
 and

I. Puerari⁴
Instituto Nacional de Astrofísica, Óptica y Electrónica, Puebla, MD 21218, México

ABSTRACT

We present a structural analysis of nearby galaxies in spiral-spiral pairs in optical *BVRI* bands and compare with the structures of isolated spiral galaxies and galaxies in ongoing mergers. We use these comparisons to determine how galaxy structure changes during galaxy interactions and mergers. We analyze light concentration (C), asymmetry (A), and clumpiness (S) parameters, and use the projections of CAS parameter space to compare these samples. We find that the CAS parameters of paired galaxies are correlated with the projected separations of the pair. For the widest and closest pairs, the CAS parameters tend to be similar to those of isolated and ongoing major mergers (ULIRGs), respectively. Our results imply that galaxy CAS morphology is a robust quantity that only changes significantly during a strong interaction or major merger. The typical time-scale for this change in our paired sample, based on dynamical friction arguments, is short, $\tau \approx 0.1 - 0.5$ Gyr. We find average enhancement factors for the spiral pair asymmetries and clumpiness values of ~ 2.2 and 1.5 . The S parameter, which is related to star formation activity, has a moderate level of enhancement suggesting that this activity in modern spirals depends more on internal processes than on external conditions.

We furthermore test the statistical criterion for picking up interacting galaxies in an automated way by using the $A - S$ projection plane. The diversity of our spiral pair sample in the CAS space suggests that structural/SF/morphological properties of interacting galaxies change abruptly only when the interaction becomes very strong and that the criteria for finding galaxies involved in major mergers from Conselice (2003) is effective.

Subject headings: Galaxies: spiral – Galaxies: structure – Galaxies: photometry – Galaxies: interactions – Galaxies: fundamental parameters – Galaxies: morphology – Galaxies: general

¹E-mail: hector@astroscu.unam.mx

²E-mail: avila@astroscu.unam.mx

³E-mail: cc@astro.caltech.edu

⁴E-mail: puerari@inaoep.mx

1. Introduction

One of the major unsolved questions in modern astronomy is understanding galaxy formation and evolution. The hierarchical clustering scenario,

motivated by the inflationary Cold Dark Matter (CDM) cosmology, has served as the main theoretical background to address this question (for a recent review see Firmani & Avila-Reese 2003). From the observational side, two types of information have been used: (i) detailed studies of local galaxies interpreted as fossil records of the formation process, and (ii) the rapidly increasing observational data of the universe at large redshifts. An important question regarding the latter item is the identification of properties which can be fairly compared among the galaxy populations at different redshifts. The correct identification and measurement of these properties is essential to infer empirically how the present-day galaxy populations formed.

Some optical morphological features along the Hubble-sequence have been used as the primary characteristic to describe local normal galaxies. Unfortunately, these features describe only the “tip of the iceberg” in galaxies. Some morphological features are thought to be related to transient internal dynamical and luminous (star formation) processes rather than to long-term fundamental physical properties of galaxies (van den Bergh 1998; Conselice 2003 and references therein). It has also been shown that gross morphological characteristics change with wavelength (Block & Puerari 1999), making it even more difficult to use them as a basis for a physical classification of galaxies. On the other hand, a high fraction of distant galaxies look peculiar and cannot be placed onto the Hubble sequence (Glazebrook et al. 1995; Abraham et al. 1996; Conselice et al. 2004) suggesting that there must be a physical cause for this change (Conselice 2003). These facts have motivated the search for quantitative physical indices, which would allow galaxies to be classified in different stages of their evolution (Bershady et al. 2000). In this spirit, the latter authors and Conselice (2003) have proposed three structural indices to distinguish galaxies at different stages of evolution, namely the concentration of stellar light (C), the asymmetry in the light distribution (A), and a measure of its clumpiness (S).

According to the galaxy formation picture based on the hierarchical CDM cosmogony, disk galaxies assembly generically inside CDM halos. The main properties of the disks are de-

termined largely by the halo mass aggregation history (and its related concentration), and by the halo angular momentum (Mo et al. 1998; Firmani & Avila-Reese 2000; van den Bosch 2000; Zavala et al. 2003). On the other hand, in the hierarchical picture, the morphological characteristics of galaxies may change several times during its evolution (Kauffmann et al. 1993; Baugh et al. 1996). Therefore, the structure of a galaxy at a given time reveals its present and past formation history. The *CAS* morphology system was designed and tested to reveal the major properties of galaxies (Conselice 2003). The C parameter is related to the scale of a galaxy (mass, size) and its halo angular momentum, in particular the spin parameter, which is roughly constant in time for most of the halos. C could slightly change (increase) with time depending on the galaxy mass accretion rate and relaxation history. Strong changes are expected only when dissipative major mergers happen (when a spheroid forms, for example). The S parameter, which traces recent star formation (SF) (Conselice et al. 2003b), is expected to change the most with time for a given galaxy as SF occurs. The SF rate history of isolated normal disk galaxies is predicted to increase smoothly, on average by a factor of 1.5 – 4, from $z = 0$ to $z \sim 1 - 2$ and then to decrease slightly at higher redshifts (1). However, interactions may abruptly enhance SF (Hernández-Toledo et al. 2001), increasing S in this case. Finally, the parameter A is expected to change significantly during interactions and mergers (Conselice et al. 2000).

The *CAS* parameters therefore may trace out fundamental physical stages of galaxy evolution, as well as possible transient processes related to interactions. In the hierarchical scenario the rate of halo major mergers increases dramatically with redshift (Gottlöber et al. 2001). Observations show that in the local universe only about 2 – 8% of galaxies are in interacting pairs (Xu & Sulentic 1991; Patton et al. 2000), but this fraction increases significantly with redshift as shown for a galaxy sample up to $z \sim 0.5$ (Patton et al. 2002). From these data and assuming short merging time scales (< 0.5 Gyr), the latter authors infer that the merging rate increases as $(1 + z)^{2.7}$. Thus, at $z \sim 3$, the merging rate would be ~ 40 times the present one. Interestingly, at $z \sim 3$ the observed fraction of

galaxies with asymmetric features typical of a recent merger was found to be as large as 50% for the most luminous and massive sources (Conselice et al. 2003a,b). The detailed study of the local interacting pairs is crucial for understanding the structures of high-redshift galaxies. In this spirit, the aim of the present paper is to study *CAS* parameters and correlations for a local sample of spirals in pairs, and compare them with the *CAS* parameters for a reference sample of non-interacting galaxies and a sample of merging galaxies, namely ultra luminous infrared galaxies (ULIRGs). This further allows us to determine what physical processes are required to change the morphologies of galaxies. We explore how different stages of interactions affect the structure, morphology, and SF properties of galaxies as revealed through *CAS* parameters. In a subsequent paper (Hernández-Toledo et al. 2005, Paper II), the correlations of the *CAS* parameters with other galaxy properties in pairs will be explored in order to gain insight on the significance of these parameters for understanding galaxy interactions and evolution.

To address these questions, we use a set of broad-band *BVRI* observations of 66 spirals in interacting pairs (Hernández-Toledo & Puerari 2001), a set of F555W/F606W and F814W HST observations for 66 ULIRGs (Conselice 2003 and references therein), as well as a comparison sample of ~ 90 bright, large non-interacting local galaxies from the catalog of Frei et al. (1996).

The structure of the paper is as follows. Section 2 summarizes the main characteristics of the samples that are relevant to this study. In § 2.4 an overview of the *CAS* parameters and their measurements is given. In Section 3 we present the *CAS* parameters in the *B*, *V*, *R* and *I* bands for the (S+S) pairs and compare their loci in the *CAS* volume with that of the reference samples of isolated galaxies and ultraluminous infrared galaxies (ULIRGs). The results are discussed and interpreted in § 4. In § 5 we present our conclusions.

2. Observations

2.1. (S+S) Pair Sample

The (S+S) sample used in this paper is a collection of 66 disk galaxies in pairs observed by Hernández-Toledo & Puerari (2001) and selected

from the Catalog of Isolated Pairs of Galaxies in the Northern Hemisphere (Karachentsev 1972). The (S+S) pairs occupy a special place among physical binaries. They represent a good laboratory from which to study secular evolution due to interactions. These pairs are also thought to be the precursors of major galaxy mergers that likely dominate the process through which massive galaxies form (Conselice et al. 2003a,b). The selection criteria applied yields a sample that is biased against the presence of mergers since only components with discernible diameters were selected. Instead, a wide range of separations and morphological features, presumably associated with tidal interactions, are present. The mean projected separation of the components in the sample is $\sim 30 h_{0.7}^{-1} \text{kpc}$, with the closest and widest systems separated by ~ 10 and $\sim 100 h_{0.7}^{-1} \text{kpc}$, respectively.

The sample is restricted to an isolated environment, where only very small neighbors are allowed around each component. From the isolation criteria, for a circle of diameter equal to the pair projected separation around each component, the apparent diameter of any possible neighbor can not exceed 1/5th the diameter of the secondary component. Smaller galaxies and/or fainter than $m_V = 15.7$ m (the limit magnitude of the sample), might be present in these pairs. Although small satellite galaxies may have some influence on the morphological (*CAS*) properties of the pair components, one expects that these properties in our sample are affected mainly by the effects of the mutual interactions between the pair components.

Hernández-Toledo & Puerari (2001) obtained deep images in the Johnson-Cousins *BVRI* photometric system with typical integration times of 40, 25, 10 and 10 minutes respectively¹. The images were acquired using two telescopes: the Guillermo Haro Observatory (GHO) 2.1m telescope at Cananea, Sonora and the Observatorio Astronómico Nacional (OAN) 1.5m telescope at San Pedro Mártir, Baja California, both in México and under reasonable seeing conditions ($\sim 1.6''$). The data are sensitive enough to detect faint stellar tidal structures. This is important in order

¹Detailed imaging of these galaxy sample can be found in the Vizier On-line Data Catalog J/A+A/379/54 associated to the Hernández-Toledo & Puerari (2001) paper

of not biasing the *CAS* estimates for a local reference sample of interacting galaxies. If a typical size of ~ 1.3 arcmin/galaxy is considered, an average number of 50 resolution elements/galaxy are reasonable enough to avoid underestimations of the *CAS* parameters. A more detailed description of the selection criteria, completeness and global optical emission properties can be found in Hernández-Toledo et al. (1999).

2.2. Frei Reference Sample

The Frei et al. (1996; hereafter (S)Frei) sample is a collection of 113 well-resolved non-interacting galaxies of all classical Hubble types whose quantitative morphological properties in the *R* band were listed in Conselice (2003, Table 1). Two telescopes were used to acquire these images; the Lowell 1.1m and the Palomar 1.5m with a typical resolution $\sim 2''$. A typical scale of ~ 3 arcmin/galaxy renders an average number of 90 resolution elements/galaxy. This is an important requisite for a local reference sample of non-interacting galaxies that we use for comparative purposes. The (S)Frei sample consists mainly of bright, high surface brightness galaxies. Hence the large population of low surface brightness or dwarf galaxies that make up the bulk of all galaxies in the local universe is under-represented. In this sense, the Frei sample is not an accurate representation of the entire local galaxy population but samples a wide enough range of luminosities and Hubble types for comparative purposes (see Bershady et al. 2000 for more details).

Figure 1 shows the morphological type and luminosity distributions of the (S+S) pair and (S)Frei samples. Morphological types are represented by a numeric code, *T*, according to the convention in the HyperLeda database²(HyperLeda). Notice that only galaxies with types latter than S0 ($T \geq 0$) were considered. The selection criteria applied to the (S+S) pairs favors the presence of bright almost equally-sized members with a luminosity distribution similar to that of the (S)Frei sample. The (S+S) pair sample also excludes, by definition, component galaxies with morphological types earlier than S0. The morphological distribution shows that the (S+S) sample is somewhat over-represented in earlier types with

respect to the (S)Frei sample, where the peak in the distribution is in the Sc types. This excess of early types in paired galaxies with respect to other samples of isolated galaxies has been reported before (Hernández-Toledo et al. 1999) and tentatively interpreted as evidence of secular or induced bulge-building.

2.3. ULIRGs

ULIRGs are thought to be galaxies in extreme interaction, or mergers (Borne et al. 2000; Canalizo & Stockton 2001). Several groups obtained *HST* images of ULIRGs in the F814W (hereafter *I*) and F555W (hereafter *V*) bands. The quantitative morphological properties of a compiled sample of 66 ULIRGs in these bands are presented in Conselice (2003). Alternative descriptions for these galaxies can be found in Ferrah et al. (2001). To compare the *CAS* values properly with the *R*-band images used for the (S)Frei sample, a quantitative morphological *k*-correction to estimate the *R*-band value for each morphological index in ULIRGs was applied, as described in Conselice (2003). Considering a typical FWHM of $\sim 0.12''$ and a scale of $\sim 20''/ULIRG$, an average number of 160 resolution elements/ULIRG is good for *CAS* estimates.

2.4. CAS and SEP Parameters

In the following, we briefly review the *CAS* parameters and discuss the reliability of measuring them in interacting galaxies.

Concentration of light (*C*): The parameter *C* can be measured quantitatively by using a single index that is calculated according to different definitions (Graham et al. 2001; Conselice 2003). The concentration index *C*, used here, is defined as the ratio of the 80% to 20% curve of growth radii (r_{80} , r_{20}), within 1.5 times the Petrosian inverted radius at $r(\eta = 0.2)$, $r_{P!}$, normalized by a logarithm:

$$C = 5 \times \log(r_{80\%}/r_{20\%}). \quad (1)$$

For a detailed description of how this parameter is computed see Bershady et al. (2000) and Conselice (2003). The concentration of light is related to the galaxy light (or stellar mass) distributions. Low (high) concentrations are expected for extended (compact) galaxies (Bershady et al. 2000; Graham et al. 2001).

²<http://leda.univ-lyon1.fr>

Asymmetry (A): The asymmetry index is defined as the number computed when a galaxy is rotated 180° from its center and then subtracted from its pre-rotated image. A summation of the absolute value intensity residuals are compared with the original galaxy intensities. A is also measured within $r_{P'}$. For a full detailed description see Conselice et al. (2000). The asymmetry index is sensitive to any feature that produces asymmetric light distributions. This includes SF, galaxy interactions/mergers, and projection effects such as dust lanes.

Clumpiness (S): Galaxies undergoing SF are very patchy and contain large amounts of light at high spatial frequency. To quantify this, the clumpiness index S is defined as the ratio of the amount of light contained in high frequency structures to the total amount of light in the galaxy within $r_{P'}$ (Conselice et al. 2003b). The S parameter, because of its morphological nature, is also sensitive to dust lanes and inclination.

SEP: The apparent projected separation in paired galaxies, x_{12} , is typically expressed in units of the primary component diameter, D_{25} , where D_{25} is the 25-mag/arcsec² isophote diameter in the B -band. Thus, a quantity $SEP = x_{12}/D_{25}$ is defined, and the (S+S) sample is sorted into wide ($SEP > 1$) and close ($SEP < 1$) pairs. Light contamination effects are expected in paired galaxies of similar diameters and $SEP \lesssim 1$ or in paired galaxies with different diameters and $SEP \ll 1$. If the light of the companion enters within the $r_{P'}$ of a given galaxy, then the observed $r_{P'}$ could be biased to a larger value, depending on the type of deformation induced to a “pre-contaminated” light profile. This will certainly affect the measured value of CAS parameters: C probably will increase (Section 4; Paper II), A , due to the obvious asymmetrical light contamination, will increase, and S will also tend to increase but probably to a lesser extent. This was indeed the case for 10 galaxies in our closest pairs, for which a correcting procedure described below was applied.

2.5. Measuring CAS Parameters

The measurement of the CAS parameters in the S+S pairs was carried out in several steps: (i) close field and overlapping stars were removed from each image; (ii) sky background was also removed from the images by fitting a polynomial

function that yielded the lowest possible residual after subtraction; (iii) the center of each galaxy was considered as the barycenter of the light distribution and the starting point for measurements (Conselice 2003); (iv) the CAS parameters for pairs with $SEP > 1$, as well as with $SEP < 1$ but where the companion galaxy is beyond 2 times the D_{25} of the primary, were estimated directly, i.e. individual components were not considered to be influenced by light contamination from the companion; (v) closest pairs (those with $SEP < 1$ and where the companion galaxy is within 1.5 times the D_{25} of the primary) are considered as light-contaminated by the companion. In these cases, a decontamination procedure consists first of building a model of the pair component a , called *modela*, by using the task BMODEL in IRAF. Then we subtract this model from the original image, creating an *image2*. From *image2*, we estimated CAS for component b . This same procedure is applied to component b to get *modelb* in order to estimate CAS for component a . BMODEL creates a model galaxy by taking into account all the information generated at the output of an isophotal analysis. Each model galaxy was generated in free-parameter mode, such that the ellipticity, the central positions (x_c, y_c) and the position angles were re-estimated at each galaxy radius. The resultant image, after subtracting a model galaxy to the original galaxy, yielded in most of the cases, traces of underlying structures. In such cases, these remaining features were masked or interpolated before measuring the CAS parameters. In one case (KPG 347), the overlapping degree makes it more than difficult to apply this procedure and thus we remove this pair from further analysis. The CAS parameters of the (S)Frei and ULIRG samples (in the R band) were taken from Conselice (2003).

3. The CAS Parameters of (S+S) Paired Galaxies

Tables 1 and 2 list the estimated CAS parameters in the B , V , R and I bands for our sample of 66 (S+S) pairs. In Figs. 2 and 3 the loci of the paired galaxies in the $A - C$, $A - S$, and $S - C$ planes are shown in the B and I bands, respectively. The data are presented into two groups: close paired galaxies with $SEP < 1$ (circles, mean projected separation $< x_{12} > \sim 23$

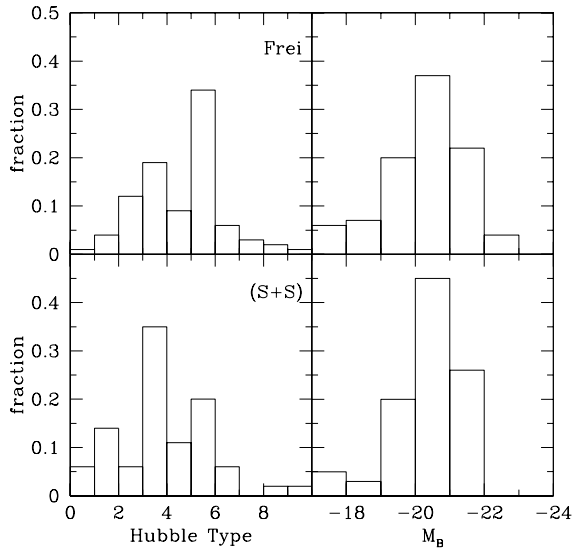


Fig. 1.— Hubble type and blue absolute magnitude distributions in the (S+S) pair and isolated (Frei et al.) galaxy samples. Morphological types have been entered as a numerical code following LEDA.

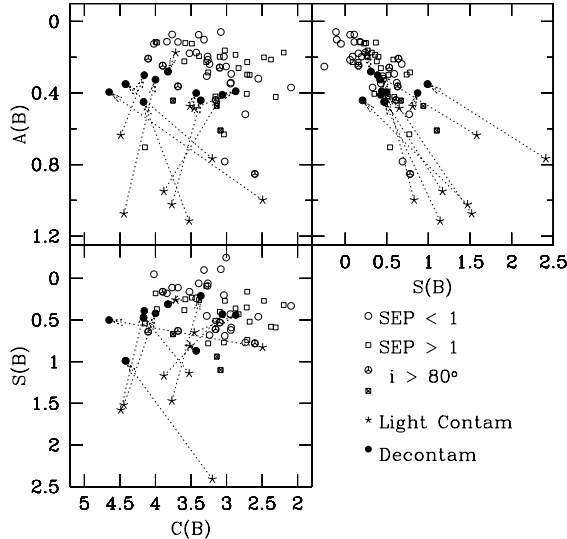


Fig. 2.— Loci of the 66 (S+S) paired galaxies in the B -band CAS planes. Different symbols are explained in the lower right panel (see text). The dashed arrows connect crude (asterisks) to decontaminated CAS values (solid circles) after applying a decontamination procedure (for the closest pairs) described in the text.

$h_{0.7}^{-1}\text{kpc}$) and wide pairs with $SEP > 1$ (squares, $\langle x_{12} \rangle \sim 46 h_{0.7}^{-1}\text{kpc}$). The trends of these two groups in the CAS space are slightly different. Asterisks show the crude (non-corrected) CAS values for the (ten) closest paired galaxies. The dashed arrows connect the crude to the decontaminated CAS values (solid circles) after applying the procedure described above. Galaxies with an inclination greater than 80° are marked with a cross.

3.1. Inclination Effects

Since high inclination could introduce a systematic biased trend in the values of the CAS parameters, it is important to evaluate its influence on the estimated parameters. Inclination to the line-of-sight is determined from the apparent flattening $\log r_{25}$ (the axis ratio of the isophote 25 mag/arcsec² in the B -band taken from HyperLeda database and morphological type T , using the classical Hubble formula $\sin^2(i) = (1 - 10^{-2} \log r_{25}) / (1 - 10^{-2} \log r_o)$, where $\log r_o = 0.43 + 0.053T$ for $-5 < T < 7$ and $\log r_o = 0.38$ for $T > 7$). In Fig. 4, the B and I band CAS parameters for the (S+S) pairs are plotted vs the inclination. The (S)Frei sample in the R band is included for comparison. A few pairs with inclinations lower than 20° could be indicating a selection effect produced by interaction distortion. However, since the corresponding number in the (S)Frei sample is low (only five galaxies), we expect no important bias in our comparison analysis. There is no significant correlation with the inclination. If any, the clumpiness parameter (S) should be slightly larger for highly inclined galaxies (see Conselice 2003). From Fig. 4 we may conclude that the uncertainty introduced by high inclination in the CAS parameters is not responsible for any significant trend in CAS space (Figs. 2, 3, 5 and 6). In any case, galaxies with inclinations larger than 80° are marked with a skeletal triangle on these plots and will not be included in the statistical calculations presented below.

3.2. Morphological Changes with Wavelength

Table 3 presents the averages and 1σ variations of the CAS parameters in the B, V, R and I bands for the whole (S+S) sample (left to the diagonal) and close ($SEP < 1$) (S+S) pairs (right to the diagonal). Galaxies with $i > 80^\circ$, and the

closest pair (KPG 347), were not included in the statistics (see §2.1). The average *CAS* parameters in different optical bands show only slight differences among them. The mean values of *A* and *S* and their variances increase towards bluer bands. A conventional statistic for measuring the significance of a difference of means (Student's T test) between the *B* and *I* bands indicates no significant differences. Alternatively, a paired TP test that takes into account point-by-point effects in the two samples indicate that the *A* parameter is significantly different at the 99 % level (against the 90 % level for the *S* parameter). However, an F test for testing the hypothesis that two samples have different variances indicates different variances in these cases. Thus caution must be taken about the interpretation of the differences in means of the *A* and *S* parameters. The *S* parameter, and in a lesser extent the *A* parameter (e.g., Conselice 2003), are related to SF activity, which is better traced by the bluer bands than by the redder ones. This hints that the observed differences in *A* and *S* may be real.

On the other hand, the average concentration *C* parameter decreases on average from *I* toward *B* bands. Since the samples show no significant difference in variances, a paired TP test supports this result at the 97 % level. It is well known that galaxy light distributions are more extended (less concentrated) in bluer bands than in red bands (de Jong 1996). However, it is possible that another effect for interacting galaxies, discussed in §4, works in the opposite direction, by increasing *C* in bluer bands. The level of change observed in the *CAS* parameters of interacting galaxies from *B* to *I* bands implies that the SF activity and morphological properties of disk galaxies are not strongly affected by the interaction, at least in periods of ~ 1 Gyr, which are larger than the typical merging time scale for these interacting galaxies.

3.3. Loci of Paired Galaxies in the Structural *CAS* Parameter Space

Figure 5 shows a comparison between (S+S) pairs and the isolated galaxy control sample in projections of *CAS* space. Since the (S)Frei sample data is only available in the *R* band, we carry out the comparison in this band. In order to avoid overcrowded diagrams, the (S)Frei data are presented in form of error bars (continuous line), cor-

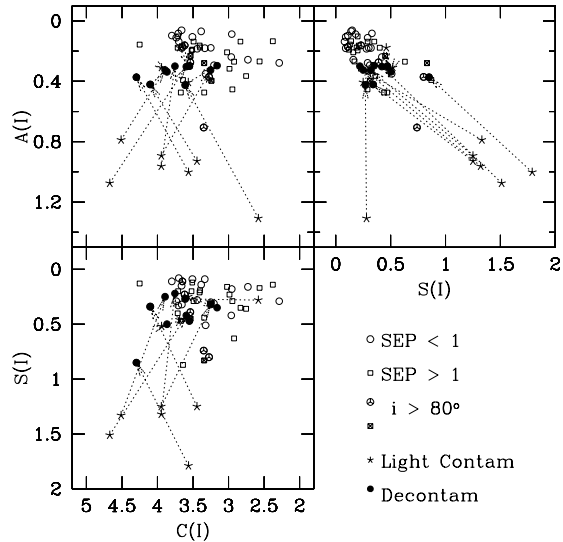


Fig. 3.— Same as in Fig. 2 but for the *I*-band.

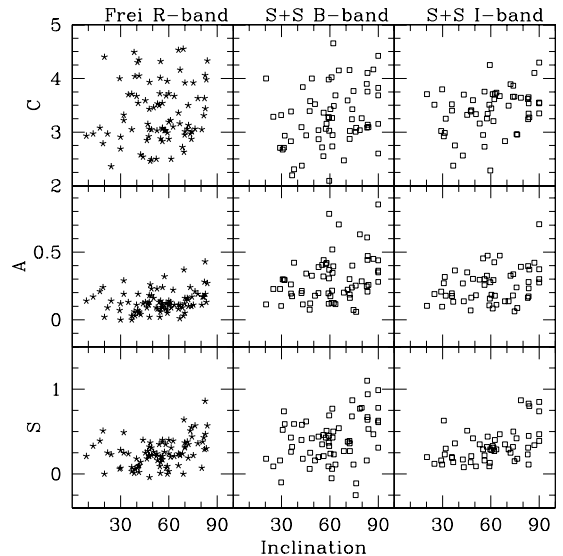


Fig. 4.— *CAS* parameters vs inclination for galaxies in the isolated (Frei et al.) and paired galaxy samples. Non-significant trends with inclination are seen for both samples in the displayed bands.

responding to the average and $1 - \sigma$ dispersion of their *CAS* parameters, binned into morphological types: Sa-Sb, Sc-Sd and Irr, from left to right in each panel, respectively (Conselice et al. 2003b). The dot-dashed error bars correspond to the average and $1 - \sigma$ dispersion of the *CAS* parameters for a sample of five prototype starburst galaxies (Conselice et al. 2003b).

3.3.1. Paired vs isolated galaxies

From Fig. 5 the loci of several galaxies in wide (S+S) pairs ($SEP > 1$, squares) nearly follow that of the isolated galaxies, while galaxies in close ($SEP < 1$, circles) pairs tend to deviate more from the isolated ones. This shows that galaxy structures, morphologies and SF activity are not strongly affected by long-term galaxy interactions or secular evolution. As a guideline for the eye, we have applied a linear regression fitting (bisector) to the (S)Frei sample data (dashed line) and the (S+S) pair sample (only $SEP < 1$ galaxies, solid line). Galaxies with $i > 80^\circ$ as well as the closest pair KPG347, were not taken into account in the fit. We used a bisector regression because we do not know a priori which are the physically independent variables in each diagram (Isobe et al. 1990). Some systematic differences can be seen: for the isolated galaxies some correlation appears in the $A - C$, $A - S$ and $S - C$ diagrams (Pearson correlation coefficients, R , of -0.48 , 0.74 , and -0.60 , respectively), while for the paired galaxies a correlation is marginally significant only in the $A - S$ diagram ($R=0.68$).

Isolated galaxies exhibit a clear tendency to be more asymmetric and patchy at lower concentration values (and later Hubble types). Paired galaxies with $SEP > 1$ (wide pairs) follow a similar trend in the $A - S$ plane, although with a larger scatter. For galaxies in close pairs ($SEP < 1$), a clearer tendency to deviate from these correlations in the $S - C$ and $A - C$ diagrams is observed, with several of the most concentrated pairs with large clumpinesses and asymmetries (see also the *B* band results in Fig. 2). In §4 we discuss possible reasons for this behavior and what could be driving the weak structural evolution in interacting galaxies.

Table 4 shows the *R* band averages and $1 \pm \sigma$ variations of the *CAS* parameters for (S+S) pairs, isolated galaxies, and ULIRGs, respectively. Addi-

tionally, averages and $1 \pm \sigma$ deviations corresponding to galaxies in close and wide ($SEP < 1$ and $SEP > 1$) pairs and ULIRGs in advanced stage of merging, i.e., excluding ULIRGs whose images still show discernible components (see below), are also presented.

The mean values of the *A* and *S* parameters for close pairs ($SEP < 1$) in the *R* band are ~ 2.2 and ~ 1.5 times larger than those for the isolated galaxies, respectively. A T test supports this result at the 99.9 and 99.8 % level, respectively. A Kolmogorov-Smirnov test also shows different distributions in the samples for both parameters at a high significance level (3.2×10^{-4} and 1.8×10^{-2} , respectively). Thus, gravitational interactions tend to increase more quickly the global asymmetry than the clumpiness, consistent with asymmetries being more sensitive to the effect of ongoing galaxy interactions/mergers (Conselice 2003). The amplitude of the observed asymmetry is consistent with the results of Iono et al. (2004) who have recently investigated the detailed response of the *C* and *A* structural parameters for both the stellar and gaseous components in different stages of a disk-disk collision. They predict an increase in the stellar asymmetry of a factor ~ 2 over a period of $\sim 7 \times 10^7$ years that is maintained in amplitude until the end of their simulations. These authors comment that the small dynamic range predicted for *A* simply reflects the intrinsic axisymmetric nature of the tidally induced features and that blindly applying the parameter *A* to examine the degree of tidal disturbance therefore can result in large uncertainties. Regarding this last point, we argue that well-selected and deeply observed samples like the S+S pairs, with a wide range of orbital parameters and morphological features, are necessary.

On the other hand, the Student's T test shows no significant difference in the means for the *C* parameter of pairs and the reference Frei sample. If we consider that in (S+S) paired galaxies, early Hubble types are overabundant with respect to the reference sample (Fig. 1), and that *C* for the reference galaxies increases in average as the type is earlier (Conselice 2003, Table 6), then higher average values of *C* in pairs than in isolated galaxies are naively expected. However, galaxy interactions could affect not only the morphological type but also the concentration parameter *C* (e.g., Iono

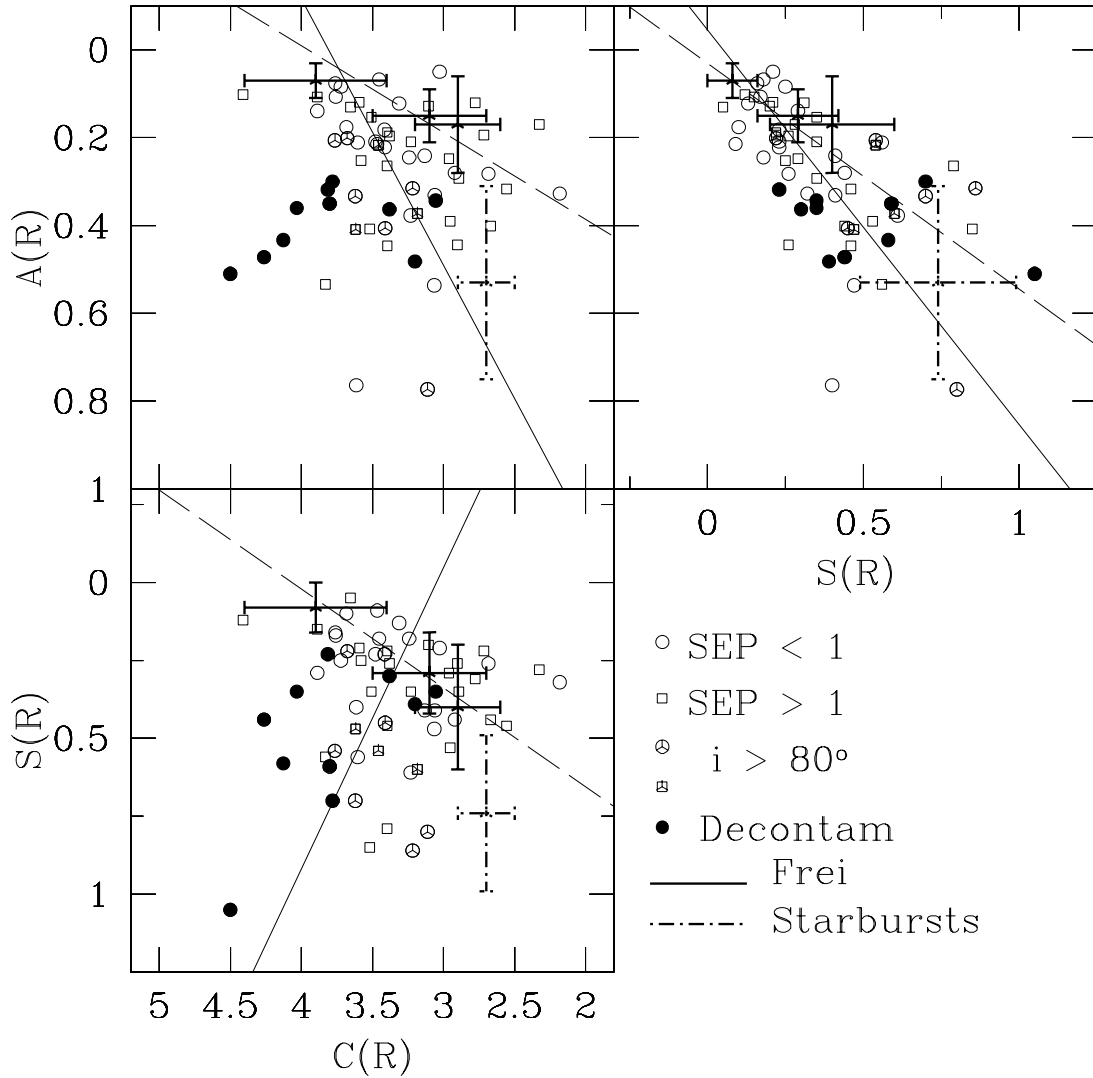


Fig. 5.— As in Fig. 2, but in the R -band and including the regions where the isolated (Frei et al.) and starbursts galaxies fall with their corresponding 1σ variations. Thick solid error bars, from left to right in each panel, correspond to the Sa-Sb, Sc-Sd, and Irr isolated galaxies, respectively. Dot-dashed error bars correspond to the starburst sample. Solid and dashed lines are the bisector linear fittings to pairs with $SEP < 1$ and isolated galaxy samples, respectively (see text)

et al. 2004), in such a way that it would not be correct to use the $C - T$ dependence of the reference galaxies for the (S+S) pairs. In fact, we find that there is some trend in paired galaxies to have higher concentrations as the parameter SEP is smaller.

3.3.2. Paired vs Ongoing Major Mergers

Figure 6 shows a comparison of the (S+S) pairs (circles and squares) and the 66 ULIRGs (ongoing major mergers, dots) (§2) in CAS structural space. Paired galaxies tend to be, on average, significantly less patchy, concentrated, and asymmetric than ULIRGs. The T test supports the differences in means for the A parameter at the 96.5 % level. However, an F test indicates significantly different variances in the C and S parameters, complicating the interpretation of these differences. A Kolmogorov-Smirnov test however, supports significant differences in the distribution of the S and A parameters at the 95 and 99 % level respectively.

Notice that ULIRGs are commonly considered as individual objects, and in consequence their CAS values were measured as such (Conselice 2003). However, from a visual examination of the HST images, we find that a fraction of the ULIRGs still show discernible components. Although a discussion on whether these objects should be considered as individuals or not is out of the scope of the present work, we identify in Fig. 6 these ULIRGs in process of merging with an extra cross. In Fig. 6 ULIRGs show larger scatter than (S+S) pairs in the three projections of the CAS space. This is supported in the C and S parameters by the results of the F test. However, an important contribution to this scatter comes namely from the ULIRGs with discernible components (crosses), especially in the S parameter.

In the $A - S$ plane several of the highly asymmetric ULIRGs tend to be more patchy than the highly asymmetric paired galaxies. If only ULIRGs with non-discernible components (ULIRGs in advanced merging process) are considered, then the differences between both samples are more dramatic in the sense that the most patchy “advanced” ULIRGs are less asymmetric than the most patchy paired galaxies. The most concentrated “advanced” ULIRGs tend to have average or lower than average A parameters, while

the more concentrated close (S+S) galaxies tend to have large A parameters (see $A - C$ plane). The most patchy “advanced” ULIRGs tend to have average or even lower than average concentrations (see $S - C$ plane), opposite to the trend observed in (S+S) galaxies.

4. Discussion

4.1. The Robustness of Morphology in the Absence of Major Merging

As we have shown, the C and A values for spirals in (S+S) pairs are on average larger than the corresponding ones to spirals in the isolated galaxy control sample. We have also shown that as the separation parameter SEP increases, the CAS values of the galaxies and their distribution in the CAS structural space tend to be closer to those for isolated galaxies. On the other hand, as SEP is smaller, the CAS parameters and their distribution in the CAS space become more similar to those of ULIRGs - ongoing major mergers. The large range of CAS values for the (S+S) pairs reveals a large diversity of dynamical stages and morphologies in these systems, consistent with the expectations from their selection criteria. A representative projected separation and relative radial velocity (averages) can be used to estimate the average merging time in close ($SEP < 1$) and wide ($SEP > 1$) pairs. Alternatively, we can use dynamical-friction time arguments for Cold Dark Matter halos to estimate merging time scales of the central galaxies, assuming circular orbits (Klypin et al. 1999). This method indicates that the average merging times for our close ($SEP < 1$, $\langle x_{12} \rangle \sim 20 h_{0.7}^{-1} \text{kpc}$) and open ($SEP > 1$, $\langle x_{12} \rangle \sim 50 h_{0.7}^{-1} \text{kpc}$) (S+S) pairs are ~ 0.15 Gyr and ~ 0.5 Gyr, respectively. Our results show that the structural/SF/morphological properties of interacting galaxies change significantly only when the interaction becomes very strong just before the merger commences; the time scale to produce these changes is of the order of the merging time, roughly 0.15-0.5 Gyr. A note of caution. These small time scales imply that the fraction of recently merged systems (c.f. luminous ellipticals) should be close to half the fraction of local paired galaxies. However, this fraction of field luminous (elliptical) galaxies seems not to be observed in the local optical luminosity function of field galaxies

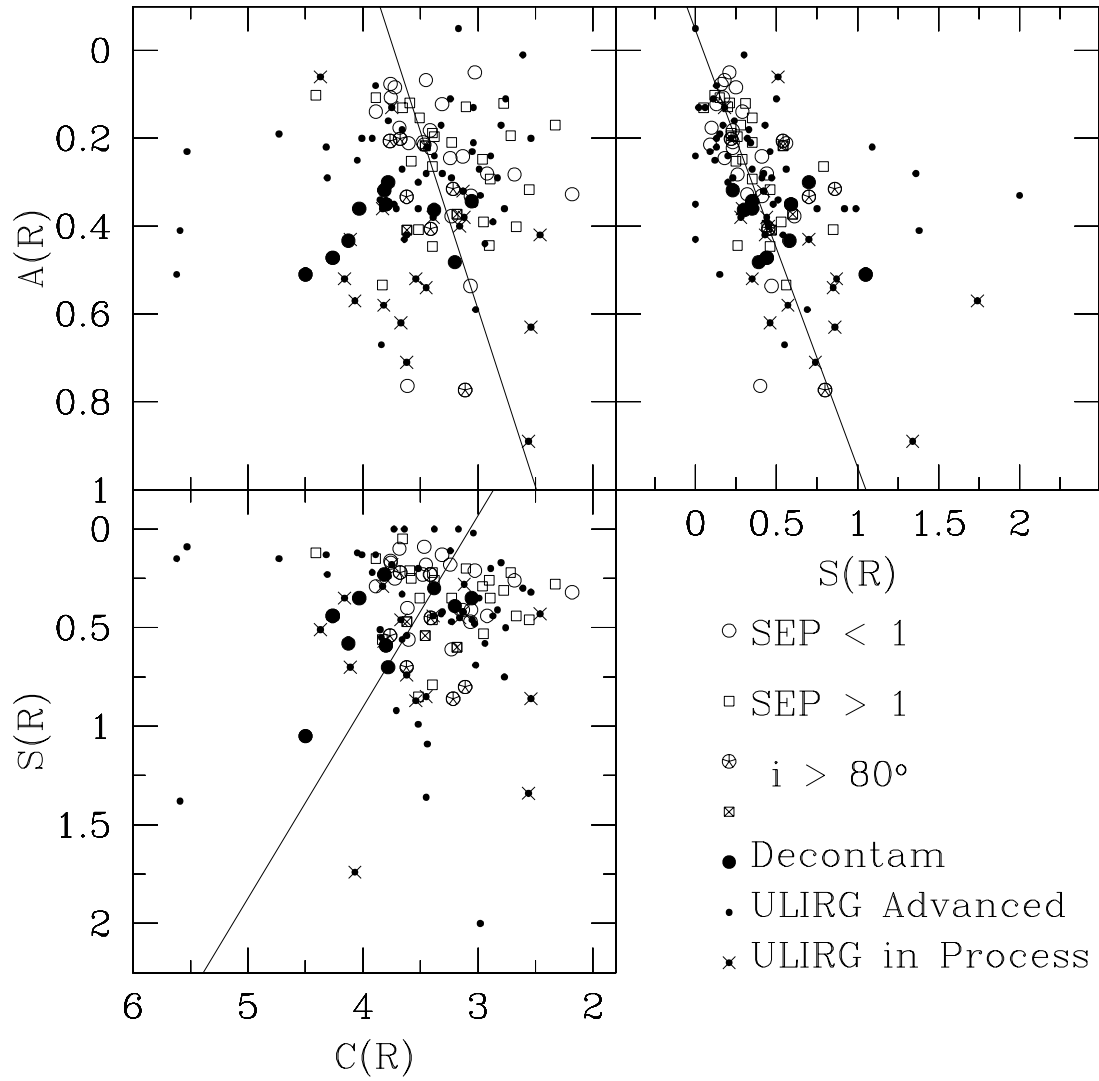


Fig. 6.— Same as Fig. 2, but in the R -band and this time including the individual points for the “advanced” ULIRGs (small-solid dots) and “in process” ULIRGs (crossed small-solid dots) sample. Solid line is the bisector linear fitting to the pairs with $SEP < 1$.

(c.f. Sulentic & Rabaca 1994; Hernández-Toledo et al. 1999).

The continuous change of the *CAS* parameters as a function of *SEP* is also shown qualitatively in Fig. 7. This figure plots the σ -deviations of the (S+S) pairs in units of the (S)Frei sample σ -deviations in the $A-C$, $A-S$, and $S-C$ planes, as a function of *SEP*. Bisector linear fittings (using the corresponding formula for the variance σ) to the isolated (S)Frei galaxies in the *CAS* planes were used as the reference relations. As the projected separation in paired galaxies decreases, the larger on average their σ -deviations from the isolated galaxy sample are. Dashed lines show the $\pm 2\sigma$ level of the fits to the reference (S)Frei sample. In general, the largest σ -deviations are in the $A-S$ diagram as expected for systems that are undergoing interactions/mergers (Conselice 2003).

Figure 8 shows the σ -deviations for (S+S) pairs versus an interaction index introduced by Karachentsev (1972). The *AT* index is designated for pairs with components in a common luminous halo with an amorphous, shredded, or asymmetric structure. *LI* pairs show evidence of tidal bridges, tails or both in discernible components. *DI* pairs show evidence of structural distortion in one or both of the separated components. Finally, a *NI* class is introduced for wide pairs with no obvious morphological distortions. The order $AT-LI-DI-NI$ has been suggested (Hernández-Toledo et al. 2001) as a sequence from strongest to weakest evidence for tidal distortion or, alternatively, most to least dynamically evolved (interpreting a common envelope as a sign of extensive dynamical evolution in pairs). The strongest σ -deviations in Fig. 8 correspond to the *AT* and *LI* galaxies in the $A-S$ diagram, while pairs belonging to *DI* and *NI* classes show less than 2σ -deviations from the reference isolated galaxies. The relative fraction of galaxies above 2σ of the reference level are 75%, 60%, 40% and 38% for *AT*, *LI*, *NI* and *DI* classes, respectively. The results in Figs. 7 and 8 are further evidence that the $A-S$ diagram can be used as an indicator for strong or dynamically evolved interactions.

4.2. Interacting Galaxies in the $A-S$ Plane and Induced Star Formation

We have discussed previously that interactions do not increase clumpiness values (*S*) as much as they do the asymmetries (*A*) of galaxies (see the trends for isolated and paired galaxies in the $A-S$ diagram of Fig. 5). According to our results, the average value of *S* for close paired galaxies is ~ 1.5 times larger than the corresponding average for isolated galaxies. This enhancement factor is similar to the average one (~ 1.6) in the optical luminosity of the late-type pair components relative to isolated galaxy control samples. This has been interpreted as the optical signature of the interaction-SF connection (e.g., Hernández-Toledo et al. 1999). All these pieces of evidence show that while the interaction level traced by the asymmetry *A* becomes significant, the interaction-induced SF rate increases only moderately in pair galaxies, suggesting that the SF activity in disk galaxies could be more related to internal processes rather than to external ones (Lambas et al. 2003). The SF rate in isolated disk galaxies varies by about a factor of ten (e.g., Kennicutt 1998).

Nevertheless, when the interaction is strong and properly corresponds to the merging phase, the *S* parameter increases significantly, as it is seen in the ULIRGs (Fig. 6; Conselice 2003). The (S+S) pairs also show a systematic increase in their σ -deviations from the reference isolated galaxies in the $A-S$ plane as *SEP* decreases (see Fig. 7). A similar trend with *SEP* was found for the $25\mu\text{m}$ -to-*B*-band (and FIR-to-*B*-band) luminosity ratio in (S+S) pairs and (E+S) pairs (Hernández-Toledo et al. 2001).

Consistent with these results, Barton et al. (2000, 2003) suggested previously that the strengths and the ages of triggered bursts of SF depend on the galaxy separation on the sky. A confrontation of their starburst models to observations indicates that the strongest bursts of SF occur only in the tightest orbits, giving rise to a burst strength-separation correlation. The burst of SF triggered by the close galaxy-galaxy pass continues and ages as the galaxies move apart. However, it is important to notice that the underlying scenario of triggered SF in the Barton et al. (2000, 2003) work is the density-driven model of SF, where the interaction induces a large central gas concentration.

Therefore, the burst of SF occurs mainly in the central regions (Mihos & Hernquist 1996). With this model it has been possible to produce starbursts comparable to those inferred in ULIRGs. Nevertheless large-scale, prompt and diverse SF activity is also seen in many interacting galaxies.

An alternative mechanism for triggered SF is the shock-induced model of SF (Jog & Salomon 1992). At odds to the density-driven model, recent simulations using the shock-induced SF (Barnes 2004) show that (i) the SF response to the interaction is immediate, the burst being produced mainly at pericenter, (ii) the SF is spatially extended because the gas is more widely distributed, (iii) the different encounter geometry may yield a variety of SF rate histories. The confrontation of observations with models of spectro-photometric evolution in Barton et al. (2003), although applied mainly to the central regions of interacting galaxies, suggests indeed that the ages and strengths of triggered bursts of SF depend on the galaxy separation. However, in the density-driven SF model such a dependence is hard to predict since the burst is delayed until the gas density has had time to build up in the center, which may happen a long time after the pericenter pass.

A corollary of item (ii) is that the surface brightness profiles in the bluer bands should become, if any, more extended than in the pre-burst galaxy, but not more concentrated. To this respect we have noted two trends in our paired sample: several of the close pairs tend to have a low average B -band surface brightness ($\langle \Sigma \rangle = L/2/\pi r_e^2$, where r_e is the effective radius), i.e. their r_e apparently became larger. On the other hand, the C parameter for these galaxies is typically high. Both effects can be explained together if the surface brightness profile increases externally, becoming shallower in the outer regions. For example, if an exponential surface brightness profile is gently flattened at the periphery (e.g., at radii $\gtrsim 80\%$ of the r_P) then the C parameter used here (§2) will increase slightly while $\langle \Sigma \rangle$ will decrease.

Probably, both the density-driven and the shock-induced mechanisms for SF, are working in galaxies, with one or the other more important in different cases, from the isolated state to the merging phase. Further theoretical and observational study will be important to clarify the mechanism of triggered SF in interacting galaxies.

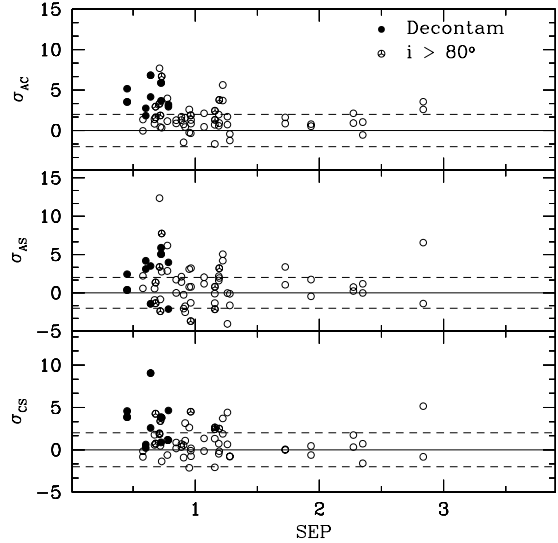


Fig. 7.— The σ -deviations of paired galaxies from the isolated ones in the R -band $A - C$, $A - S$, and $S - C$ planes vs SEP , by taking as reference a bisector linear fit to the isolated galaxies. Dashed lines indicate the $\pm 2\sigma$ deviations.

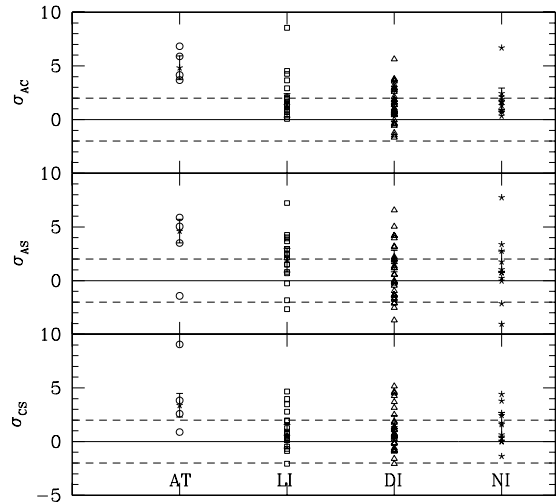


Fig. 8.— Same as in Fig. 7, but vs the interaction class indices. The indices AT, LI, DI and NI characterize a sequence from strongest to weakest evidence of dynamical interaction (see text for an explanation of how is assigned this index to each pair galaxy).

In conclusion, from our study of the *CAS* parameters for a sample of local paired galaxies we find that the parameter S , which directly correlates with SF activity (Conselice 2003), increases systematically with decreasing projected separation (in the plane of the sky), but this increasing is typically moderate. We also find that the concentration parameter C in optical bands tends to be high for the most asymmetric and patchy paired galaxies, opposite to the tendency of isolated galaxies. This could be due to either a significant increasing of the central surface brightness in the interacting galaxy or to a flattening at the outskirts of its surface brightness profile. In the former case one expects that the effective radius will decrease and $\langle \Sigma \rangle$ will increase. This topic will be carefully analyzed elsewhere (Paper II). In the following, we discuss some possibilities that could produce a flattening of a surface brightness profile at the outskirts in an interacting galaxy.

4.3. Concentration Parameter

In §3 we have shown that some galaxies in close pairs exhibit an inverse tendency with respect to isolated galaxies in the $A - C$ and $S - C$ planes: their C tend to be high for large clumpiness and asymmetry parameters (see Fig. 5). These results suggest that close interactions may increase the concentration parameter of disks. As discussed in §4.2, the C parameter is sensitive to changes in both the outer ($r > r_{80}$) surface brightness profile and the inner ($r < r_{20}$) one. In the former case, a higher value of C could be due to either (a) an outer flattening of the surface brightness profile (see §4.2) or (b) a dynamical expansion of the outer disk.

In case (a), the flattening may be produced by a light contamination effect or by an induced physical process in a galaxy disk. Notice that we have mostly taken into account the contamination after applying a correction procedure described in §2.1. A physical process related to interactions that could flatten the outer optical-band surface brightness profile is the shock-induced model of SF bursts due to interactions mentioned in §4.2. Since the gas surface density distribution of local galaxies is typically much more extended than the stellar surface density (and with lower values in the central regions), the distribution of the young stars, product of the shock-induced burst of SF,

will also tend to be extended and with a *fractional* contribution to the corresponding (pre-burst) surface brightness more significant at the periphery than in the central regions (the gas surface density in local disk galaxies is typically even higher than the stellar one at the periphery). However, it should also be considered that differential rotation may decrease the molecular/neutral cloud formation in the periphery. Nevertheless, recent numerical simulations of shock-induced SF (instead of density-driven SF) for an observed interacting galaxy tend to confirm that SF is induced along the whole disk (Barnes 2004).

In case (b), Iono et al (2004) have predicted, from numerical simulations of disk-disk collisions, a measurable change of the parameter C . They have found that C is more sensitive to the behavior of r_{80} than to r_{20} , because for the inner regions, the stars respond to the collision with significantly smaller amplitudes. It could also be that due to the interaction the disk suffers bar instabilities and, in this case along with bulge formation, the outer disk expands significantly (Valenzuela & Klypin 2003). Thus, the predicted increasing of C is the result of a) the ejection of the outer stars into tidal tails and b) a rapid expansion of the stellar disk outside the tidal radius.

4.4. Identifying Strong Interactions with *CAS* Parameters

By using a sample of ongoing major mergers (the same ULIRG sample used here), Conselice (2003) established a criterion for recognizing merging galaxies: $|A - \bar{A}_{\text{isol}}| > 3\sigma$, where $(A - \bar{A}_{\text{isol}})$ is the residual of the observed value with respect to a linear fitting to the sample of isolated galaxies in the $A - S$ plane. In the case of pairs, according to Fig. 7 approximately 55% (40%) of the paired galaxies are above the $\pm 2\sigma$ ($\pm 3\sigma$) level in this plane. Two thirds of them have $SEP < 1$ and most of the them have clear morphological signatures of strong interactions (i.e., tails, bridges, distortions). In Fig. 8 one sees that most of the interacting galaxies (AT and LI interaction classes) are above the $\sim 2\sigma$ level in the $A - S$ plane. Therefore the criterion $|A - \bar{A}_{\text{isol}}| > 2\sigma$ for paired interacting galaxies in the $A - S$ plane seems to be *statistically* adequate to identify these systems in an automated way.

On the other hand, we find that the devia-

tions of the paired galaxies in $A - S$ space are slightly different to the pattern seen for ULIRGs (see Fig. 6, where ULIRGs are more scattered than pairs, and with a tendency to increase S steeply with A than the paired galaxies). The major differences in the $A - S$ diagram are found for “advanced” ULIRGs; the A parameter in this case is relatively small for the large values of the S parameter, which trace the SF rate. Nevertheless, even in these cases, the ULIRG SF rate traced by the optical S parameter is much smaller than the one inferred from the FIR emission.

Finally, we notice that a merging limit criterion based only on the asymmetry parameter ($A > 0.35$ for example, Conselice et al. 2003a; Conselice, Chapman & Windhorst 2003b) should be complemented with the σ_{AS} -deviation criterion when possible. In Fig. 9, σ_{AS} is plotted versus A . There are several paired galaxies with $A < 0.35$ but with deviations $|A - \bar{A}_{\text{isol}}| > 2\sigma$, that are in fact interacting. Paired galaxies with $A > 0.35$, almost invariably deviate from the isolated ones by more than $\pm 2\sigma$.

4.5. High Redshift Galaxy Morphology

A goal behind the introduction of the CAS system is the evaluation of the structural and morphological evolution of galaxies. There is mounting evidence that the population of unobscured star-forming galaxies has dramatically changed around $z \sim 1 - 2$: at higher redshifts, the galaxy population was dominated by peculiar galaxies, while at lower redshifts, most of galaxies are already “normal” spirals and ellipticals (Conselice, Blackburne & Papovich 2004, and references therein). The latter authors have measured the rest-frame B -band CAS parameters for a large sample of field galaxies in the Hubble Deep field North and South (HDF-N & S) out to $z \sim 3$. The high-redshift galaxies ($z \gtrsim 2$), which are mostly peculiars, show a clear deviation from the field low-redshift galaxies in the $A - C$ and $A - S$ diagrams. An interesting question is whether the CAS parameters of these high-redshift peculiars look similar to those of the local interacting galaxies.

The high-redshift peculiar galaxies from Conselice et al. (2004) occupy the $A - S$ plane (see their Fig. 19) with values of A and especially of S , much smaller on average than those of our local

sample of pair (S+S) galaxies. One expects some systematic under-estimating of S and A with redshift for disks due to resolution effects (see Fig. 16 in Conselice et al. 2003b, and Table 1 in Conselice et al. 2004). Taking into account these effects, the loci of the HDF-NS peculiar galaxies with redshifts higher than ~ 2 in the $A - S$ plane become closer to the location of our local pairs. However, it is difficult to identify both families of objects in the $A - C$ plane as likely similar. The high-redshift peculiars have concentrations smaller on average than the local pair galaxies. The resolution effect for the high-redshift disks does not affect significantly the C parameter. Thus, according to the CAS system, a preliminary statement is that most of the HDF high-redshift peculiars are similar to local starburst galaxies rather than to our whole sample of local pair (S+S) galaxies. Of course, there is an overlapping in the CAS space of both group of galaxies (Fig. 5), reflecting the fact that some starburst galaxies originate in interacting systems. It should also be taken into account that galaxies at high-redshifts are much more gas rich than the present ones. A more careful comparison and interpretation of local and high-redshift galaxies based on the CAS system will be presented elsewhere.

5. Conclusions

We have measured CAS parameters in $BVRI$ bands for a sample of 66 galaxies in (S+S) pairs (Hernández-Toledo & Puerari 2001) and carried out a comparison analysis in two steps: 1) an inter-band internal comparison of the CAS parameters in (S+S) pairs and 2) an R band comparison in the CAS structural space among (S+S) pairs and two samples with similarly compiled parameters, the (S)Frei control sample of isolated galaxies and 66 ultraluminous infrared galaxies (Conselice et al. 2003b). This has allowed us to gain insight on how morphology and SF changes as a function of interaction/mergers and recognize time-scales and physical effects that drive the evolution of these galaxy features. Our main conclusions are as follow:

(i) The differences in CAS parameters for paired galaxies from the B to I bands is in general and on average small, suggesting that the optical CAS parameters are stable galaxy properties until the

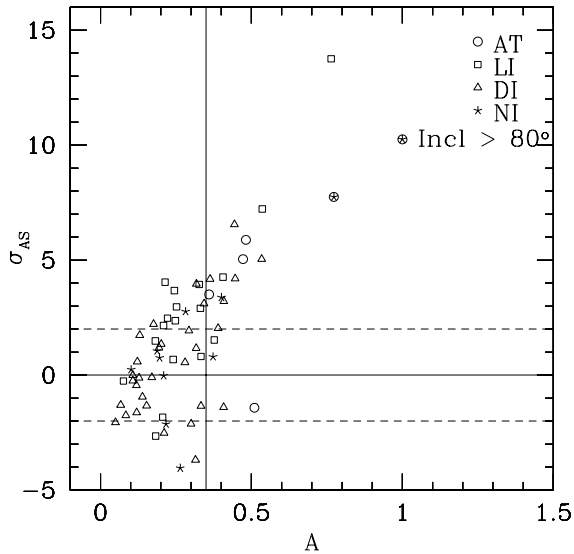


Fig. 9.— The σ -deviations of paired galaxies from the isolated ones in the $A - S$ plane vs A . Two interaction criteria are illustrated: $A > 0.35$ (right to the solid line) and $|A - \bar{A}_{\text{isol}}| > 2\sigma$ (out from the dashed line region). The agreement between both criteria is good except for some galaxies for which $A < 0.35$ but $|A - \bar{A}_{\text{isol}}| > 2\sigma$. These galaxies belong in fact to the LI and DI interaction classes.

beginning of a strong interaction. The average concentration C parameter decreases on average from I to B bands, consistent with the finding that galaxy light distributions are more extended (less concentrated) in bluer bands than in red bands (de Jong 1996).

(ii) The CAS parameters of paired galaxies change depending on the separation parameter SEP , in the sense that the CAS parameters for the widest and closest paired galaxies tend to be closer to those of isolated and ongoing major mergers (ULIR) galaxies, respectively. The mean values of the A and S parameters of the closest ($SEP < 1$) paired galaxies are 2.2 and 1.5 times larger than those of the isolated galaxies, respectively, i.e., even in strongly interacting galaxies, the SF activity (related to S) does not increase too much, suggesting that this activity is more related to internal processes rather than external ones.

The deviations in the CAS planes of pair galaxies with respect to the isolated ones increase significantly on average (more than 2σ) only for the closest galaxies and those galaxies with clear interaction signatures (Figs. 7 and 8). Nevertheless, there are also paired galaxies with $SEP < 1$ but within the 2σ deviations, and pairs with $SEP > 1$ but with deviations larger than 2σ . This diversity suggests that galaxies in our sample of (S+S) pairs are in different dynamical and morphological stages, from non-interacting to strong interacting, where the projected separation SEP is only an approximate (statistical) criterion of interaction.

(iii) Trends in CAS space for the interacting galaxies differ from trends seen between CAS values of isolated galaxies. Within isolated systems lower concentration values (C) correlate with larger A and S parameters. For galaxies in close pairs, these trends disappear and even revert for the most interacting galaxies: for several of them the larger A and S , the higher is C . The concentration index for strongly interacting galaxies may become higher owing to a “flattening” in the outer surface-brightness profile produced by interaction-induced *extended* SF. In the $A - S$ plane, paired galaxies, in particular the closer ones, increase their A with increasing S more steeply than isolated galaxies.

(iv) On average paired galaxies are slightly less concentrated, asymmetric, and patchy than ULIRGs, the significant difference being in the clumpiness. The latter display also a (statisti-

cally significant) larger scatter in the CAS planes than the former. The major difference in trends between paired and ULIRG galaxies is in the $A - S$ plane: the most patchy ULIRGs have smaller asymmetries and slightly lower concentrations than the most patchy paired galaxies. The structural/SF/morphological properties of interacting galaxies change significantly only when the interaction becomes very strong.

(v) A criterion for picking up interacting galaxies that is based only on $A > 0.35$ is marginally acceptable for paired galaxies. In fact there are some interacting galaxies with $A < 0.35$. A more robust *statistical* criterion uses both the A and S parameters: $|A - \bar{A}_{\text{isol}}| > 2\sigma$, where $(A - \bar{A}_{\text{isol}})$ is the deviation of the interacting-galaxy A parameter from the predicted one from the linear regression to the isolated sample in the $A - S$ diagram, and σ is the scatter of this fitting. For ongoing major mergers (ULIRGs) the $A > 0.35$ criteria is suitable.

The summary of this work is that the quantitative structural and SF parameters of galaxies seem to change significantly only during the strong interaction/merger phases and within ~ 0.2 - 0.5 Gyr. The use of the CAS parameters to establish criteria for finding galaxies in strong interaction at high-redshift galaxies appears to hold up as it depends strongly on interaction stage (e.g., Conselice et al. 2003a,b) and changes quickly with time. Within the local sample of (S+S) pairs analyzed here, we find the entire range of structural types are represented from isolated-like structural indices to indices closer to ongoing major mergers. This suggests that morphology is a fairly robust quantify that tends to change rapidly within the major merger process on the order of hundreds of Myrs.

We thank the referee for his(her) comments and suggestions that greatly improved the manuscript. Partial support for this work was provided by CONACyT grant 33776-E to V.A. and CONACyT grant 42810/A-1 to H.H-T. C.J.C. acknowledges support from an NSF Astronomy and Astrophysics Fellowship.

REFERENCES

- Abraham, R. G., Tranvir, N. R., Santiago, B. X., Ellis, R. S., Glazebrook, K., van den Bergh, S. 1996, MNRAS, 279, L47
- Avila-Reese, V., Firmani, C. 2000, RevMexAA, 36, 23
- Avila-Reese, V., Firmani, C., Vázquez-Semadeni, E. 2003, in "Galaxy Evolution: Theory and Observations", Eds. Avila-Reese et al., RevMexAA (SC), vol. 17, p. 66
- Barnes, J.E. 2004, preprint (astro-ph/0402248)
- Barton, E. J., Geller, M. J. & Kenyon, S. J. 2000, ApJ, 530, 660.
- . 2003, ApJ, 582, 668
- Baugh, C.M., Cole, S., & Frenk, C.S. 1996, MNRAS, 283, 136
- Bershady, M. A., Jangren, A., Conselice, C. J. 2000, AJ, 119, 2645
- Block, D., Puerari, I. 1999, A&A, 342, 627
- Borne, K. D., Bushouse, H., Lucas, R.A., Colina, L. 2000, ApJ, 529, L77.
- Canalizo, G., Stockton, A. 2001, ApJ, 555, 719.
- Conselice, C. J. 2003, ApJS147, 1
- Conselice, C. J., Bershady, M. A., Jangren, A. 2000, ApJ, 529, 886
- Conselice, C., Chapman, S. C. & Windhorst, R. A. 2003, ApJ, 596, L5
- Conselice, C.J., Bershady, M.A., Dickinson, M.A., & Papovich, C. 2003, AJ, 126, 1183
- Conselice, C.J., Blackburne, J., Papovich, C. 2004, astro-ph/0405001
- Dalcanton, J.J., Spergel, D.N., & Summers, F.J. 1997, ApJ, 482, 659
- de Jong, R.S. 1996, A&A, 313, 45
- Ferrah, D. et al. 2001, MNRAS, 326, 1333.
- Firmani, C., & Avila-Reese, V. 2000, MNRAS, 315, 457

- . 2003, in "Galaxy Evolution: Theory and Observations", Eds. Avila-Reese et al., *RevMexAA (SC)*, vol. 17, p. 109
- Frei, Z., Guhathakurta, P., Gunn, J. E., Tyson, J. A. 1996, *AJ*, 111, 174
- Glazebrook, K., Ellis, R., Santiago, B., Griffiths, R. 1995, *MNRAS*, 275, L19
- Gottlöber, S., Klypin, A., & Kravtsov, A.V. 2001, *ApJ*, 546, 223
- Graham, A. W., Trujillo, I., Caon, N. 2001, *AJ*, 122, 1707
- Hernández-Toledo, H. M., Dultzin-Hacyan, D., González, J. J., Sulentic, J. W. 1999, *AJ*118, 108.
- Hernández-Toledo, H. M., Dultzin-Hacyan, D., Sulentic, J. W. 2001, *AJ*121, 108.
- Hernández-Toledo, H. M., Puerari, I. 2001, *A&A*, 379, 54
- Hernández-Toledo, H. M., Avila-Reese, V., Conselice, C. J., Puerari, I. 2004 in preparation.
- Iono, D., Yun, S. Min., Mihos, C. 2004, preprint (astro-ph/0407609)
- Isobe, T., Feigelson, E. D., Akritas, M. G., Babu, G. J. 1990, *ApJ*, 364, 104
- Jog, C. J., Solomon, P. M. 1992, *ApJ*, 387, 152
- Karachentsev, I. 1972, *Comm. Spec. Ap. Obs., USSR*, 7, 1
- Kauffmann, White, S. D.M., Guiderdoni, B. 1993, *MNRAS*, 264, 201
- Kennicutt, R. C. 1998, *ApJ*, 498, 541
- Klypin, A., Gottlöber, S., Kravtsov, A. V. & Khokhlov, A. M. 1999, *ApJ*, 516, 530
- Lambas, D. G., Tissera, P. B., Sol Alonso, M., Coldwell, G. 2003, *MNRAS*, 346, 1189
- Mihos, J.C., Hernquist, L. 1996, *ApJ*, 464, 641
- Mo, Mao, White, S. D. 1998, *MNRAS*, 295, 319
- Patton, D. R., Carlberg, R. G., Marzke, R. O., Pritchet, C. J., da Costa, L. N. & Pellegrini, P. S. 2000, *ApJ*, 536, 153
- Patton, D.R. et al. 2002, *ApJ*, 565, 208
- Sulentic, J. W., & Rabaca, C. R. 1994, *ApJ*, 429, 531
- Valenzuela, O., Klypin, A. 2003, *MNRAS*, 345, 406
- van den Bergh, S. 1998, *Galaxy Morphology and Classification* (Cambridge: Cambridge Univ. Press)
- van den Bosch 2000, *ApJ* 530, 17
- Xu, C., Sulentic, J. W. 1991, *ApJ*, 374, 407
- Zavala, J., Avila-Reese, V., Hernández-Toledo, H. & Firmani, C. 2003, *å*, 412, 633

TABLE 1
CAS PARAMETERS IN *B* AND *V* FOR (S+S) GALAXIES.

KPG	<i>B</i> -band			<i>S</i>	<i>V</i> -band		
	M_B	<i>C</i>	<i>A</i>		<i>C</i>	<i>A</i>	<i>S</i>
KPG64a	-21.44	3.02±0.12	0.78±0.01	0.69±0.03	3.41±0.14	0.80±0.01	0.86±0.03
KPG64b	-20.78	3.15±0.22	0.43±0.02	0.61±0.03	3.46±0.21	0.47±0.02	0.76±0.04
KPG68a	-21.40	2.87±0.13	0.39±0.02	0.44±0.02	2.97±0.10	0.29±0.01	0.41±0.04
KPG68b	-20.43	4.65±0.09	0.40±0.05	0.50±0.03	4.35±0.04	0.29±0.02	0.50±0.06
KPG75a	-20.31	4.02±0.44	0.12±0.00	-0.05±0.00	3.80±0.47	0.09±0.00	0.25±0.00
KPG75b	-20.11	3.00±0.23	0.25±0.03	-0.25±0.01	3.02±0.26	0.30±0.00	0.46±0.01
KPG88a	-21.04	2.71±0.12	0.29±0.05	0.74±0.04	2.82±0.12	0.37±0.01	0.55±0.01
KPG88b	-20.02	2.37±0.21	0.21±0.04	0.58±0.03	2.44±0.22	0.29±0.01	0.39±0.01
KPG98a	-20.74	2.47±0.21	0.20±0.04	0.27±0.02	2.63±0.21	0.23±0.01	0.39±0.01
KPG98b	-20.34	3.99±0.44	0.11±0.01	0.18±0.01	4.02±0.42	0.15±0.00	0.13±0.00
KPG102a	-20.66	3.26±0.48	0.21±0.01	0.06±0.00	3.54±0.54	0.29±0.00	0.18±0.00
KPG102b	-21.28	3.03±0.26	0.19±0.02	0.20±0.01	3.29±0.32	0.21±0.00	0.30±0.00
KPG103a	-20.66	3.48±0.44	0.12±0.03	0.23±0.01	3.49±0.48	0.16±0.01	0.17±0.00
KPG103b	-21.13	3.57±0.61	0.12±0.00	0.25±0.00	3.58±0.62	0.17±0.00	0.20±0.00
KPG108a	-20.28	3.08±0.17	0.60±0.04	1.10±0.04	3.08±0.19	0.42±0.01	0.44±0.01
KPG108b	-19.77	3.13±0.11	0.47±0.03	0.94±0.03	3.31±0.15	0.28±0.01	0.53±0.01
KPG112a	-19.80	3.83±0.45	0.28±0.00	0.31±0.00	3.81±0.51	0.15±0.00	0.19±0.00
KPG112b	-19.84	4.00±0.42	0.33±0.00	0.42±0.01	4.15±0.20	0.40±0.00	0.50±0.01
KPG125a	-21.02	3.38±0.31	0.19±0.01	0.26±0.00	3.46±0.31	0.19±0.00	0.26±0.00
KPG125b	-21.54	2.30±0.13	0.42±0.02	0.59±0.01	2.55±0.14	0.40±0.00	0.51±0.01
KPG136a	-21.58	2.70±0.30	0.22±0.01	0.16±0.00	2.82±0.35	0.25±0.01	0.20±0.00
KPG136b	-21.08	3.28±0.28	0.22±0.01	0.09±0.00	3.33±0.32	0.23±0.01	0.23±0.00
KPG141a	-20.46	3.03±0.13	0.63±0.03	0.77±0.03	3.45±0.15	0.47±0.01	1.17±0.02
KPG141b	-20.15	2.71±0.28	0.40±0.01	0.35±0.01	2.82±0.29	0.41±0.00	0.32±0.00
KPG150a	-20.42	3.97±0.24	0.11±0.01	0.37±0.01	4.27±0.29	0.16±0.00	0.16±0.00
KPG150b	-21.25	2.83±0.10	0.26±0.01	0.43±0.01	3.15±0.12	0.25±0.00	0.27±0.01
KPG151a	...	4.42±0.16	0.35±0.07	1.0 ±0.04	4.50±0.09	0.25±0.01	0.95±0.02
KPG151b	-20.79	4.16±0.25	0.30±0.02	0.40±0.01	3.97±0.17	0.30±0.01	0.50±0.01
KPG156a	-21.13	2.97±0.10	0.36±0.02	0.43±0.02	2.98±0.12	0.31±0.01	0.56±0.01
KPG156b	-19.68	3.49±0.29	0.20±0.01	0.23±0.01	3.41±0.31	0.18±0.00	0.31±0.00
KPG159a	-19.70	2.87±0.50	0.18±0.01	0.36±0.80	3.02±0.48	0.09±0.01	0.25±0.31
KPG159b	-20.51	3.02±0.26	0.16±0.01	0.27±0.57	3.26±0.29	0.12±0.00	0.21±0.21
KPG160a	-20.12	3.39±0.21	0.07±0.01	0.06±0.00	3.40±0.21	0.07±0.00	0.16±0.00
KPG160b	-19.28	3.09±0.22	0.25±0.02	0.53±0.02	3.14±0.24	0.32±0.01	0.79±0.02
KPG168a	-20.17	3.76±0.29	0.07±0.00	0.11±0.00	3.81±0.32	0.09±0.00	0.14±0.00
KPG168b	-17.85	4.10±0.24	0.20±0.03	0.64±0.03	2.04±0.02	0.97±0.00	0.10±0.00
KPG195a	-19.61	3.89±0.37	0.24±0.00	0.16±0.00	3.72±0.36	0.22±0.00	0.11±0.00
KPG195b	-19.26	3.68±0.20	0.36±0.02	0.63±0.02	3.60±0.22	0.31±0.01	0.59±0.02
KPG211a	-20.86	3.31±0.17	0.10±0.01	-0.10±0.00	3.72±0.20	0.10±0.00	0.03±0.00

TABLE 1—*Continued*

KPG	<i>B</i> -band			<i>S</i>	<i>V</i> -band		
	M_B	<i>C</i>	<i>A</i>		<i>C</i>	<i>A</i>	<i>S</i>
KPG211b	...	3.08±0.36	0.05±0.01	-0.11±0.01	3.17±0.38	0.05±0.00	0.08±0.00
KPG216a	-18.34	4.15±0.14	0.70±0.02	0.54±0.02	4.56±0.12	0.74±0.01	0.65±0.01
KPG216b	-19.20	3.15±0.14	0.42±0.01	0.51±0.02	3.36±0.14	0.47±0.00	0.49±0.01
KPG249a	-20.18	3.06±0.15	0.41±0.00	0.43±0.01	3.01±0.09	0.46±0.00	0.53±0.01
KPG249b	-20.35	4.17±0.21	0.45±0.01	0.47±0.01	4.08±0.07	0.55±0.01	0.45±0.01
KPG295a	-19.74	3.36±0.17	0.44±0.01	0.21±0.02	3.58±0.08	0.35±0.01	0.30±0.02
KPG295b	-20.20	3.43±0.15	0.40±0.01	0.87±0.01	3.70±0.16	0.42±0.01	0.79±0.01
KPG302a	-20.33	2.93±0.08	0.29±0.00	0.59±0.01	3.10±0.09	0.25±0.00	0.44±0.01
KPG302b	-17.24	3.52±0.21	0.17±0.01	0.16±0.01	3.52±0.19	0.20±0.01	0.20±0.01
KPG313a	-17.99	2.19±0.08	0.17±0.01	0.32±0.02	2.26±0.08	0.17±0.00	0.26±0.01
KPG313b	-18.14	3.59±0.17	0.22±0.00	0.38±0.01	3.48±0.19	0.19±0.00	0.40±0.00
KPG332a	-19.78	2.55±0.08	0.32±0.01	0.46±0.01	2.61±0.08	0.31±0.00	0.36±0.00
KPG332b	-20.15	2.60±0.03	0.85±0.01	0.78±0.02	2.92±0.03	0.83±0.00	0.90±0.01
KPG347a	-20.87	2.69±0.07	0.73±0.03	0.50±0.01	2.74±0.05	0.50±0.00	0.45±0.01
KPG347b	-21.65	2.85±0.07	0.49±0.04	0.50±0.01	2.99±0.05	0.35±0.00	0.50±0.01
KPG389a	-21.94	2.09±0.19	0.36±0.00	0.33±0.01	2.20±0.21	0.35±0.00	0.31±0.00
KPG389b	-21.49	2.93±0.17	0.34±0.01	0.62±0.01	3.13±0.19	0.35±0.00	0.60±0.00
KPG396a	-20.59	3.75±0.13	0.44±0.03	0.67±0.03	3.67±0.15	0.46±0.01	0.62±0.01
KPG396b	-19.55	2.67±0.13	0.29±0.01	0.52±0.02	2.79±0.14	0.30±0.01	0.42±0.01
KPG404a	-20.29	3.27±0.37	0.30±0.00	0.45±0.01	3.21±0.42	0.26±0.00	0.11±0.00
KPG404b	-21.97	2.73±0.09	0.51±0.01	0.77±0.03	2.95±0.10	0.49±0.00	0.54±0.01
KPG426a	-21.15	3.26±0.22	0.19±0.02	0.09±0.00	3.21±0.27	0.14±0.00	0.16±0.00
KPG426b	-20.54	3.84±0.51	0.11±0.00	0.18±0.00	3.76±0.54	0.13±0.00	0.12±0.00
KPG440a	-19.08	3.09±0.09	0.19±0.02	0.40±0.02	3.18±0.09	0.14±0.01	0.30±0.01
KPG440b	-20.79	3.25±0.08	0.28±0.01	0.78±0.02	3.32±0.08	0.27±0.00	0.80±0.01
KPG455a	-20.98	3.68±0.30	0.11±0.01	0.11±0.00	3.80±0.33	0.09±0.00	0.19±0.00
KPG455b	-21.97	3.24±0.12	0.23±0.03	0.68±0.02	3.46±0.15	0.23±0.01	0.62±0.01

TABLE 2
CAS PARAMETERS IN R AND I FOR (S+S) GALAXIES.

KPG	R -band			I -band			
	SEP	C	A	S	C	A	S
KPG64a	0.712	3.61±0.16	0.76±0.02	0.40±0.02	3.80±0.17	0.67±0.02	0.40±0.01
KPG64b	...	3.41±0.26	0.40±0.03	0.45±0.02
KPG68a	0.602	3.05±0.15	0.34±0.00	0.35±0.02	3.16±0.17	0.30±0.00	0.35±0.01
KPG68b	...	3.38±0.19	0.36±0.00	0.30±0.03	3.61±0.19	0.43±0.01	0.27±0.01
KPG75a	0.672	3.88±0.48	0.13±0.00	0.29±0.00	3.70±0.45	0.08±0.00	0.33±0.00
KPG75b	...	2.92±0.26	0.28±0.00	0.44±0.01	2.96±0.25	0.23±0.00	0.42±0.01
KPG88a	1.070	2.95±0.13	0.39±0.00	0.53±0.01	2.98±0.13	0.31±0.00	0.23±0.00
KPG88b	...	2.55±0.22	0.31±0.00	0.46±0.00	2.56±0.22	0.26±0.00	0.17±0.00
KPG98a	2.348	2.71±0.22	0.19±0.01	0.22±0.01	2.83±0.22	0.13±0.02	0.35±0.01
KPG98b	...	3.88±0.39	0.10±0.00	0.15±0.00	3.70±0.36	0.10±0.00	0.20±0.00
KPG102a	0.965	3.46±0.52	0.21±0.00	0.09±0.00
KPG102b	...	3.41±0.34	0.18±0.00	0.23±0.00
KPG103a	1.932	3.65±0.52	0.13±0.01	0.05±0.00	3.71±0.49	0.17±0.01	0.40±0.01
KPG103b	...	3.59±0.62	0.11±0.00	0.21±0.00	3.40±0.57	0.16±0.00	0.21±0.00
KPG108a	1.159	3.18±0.20	0.37±0.01	0.60±0.01	3.24±0.22	0.39±0.01	0.31±0.01
KPG108b	...	3.45±0.17	0.21±0.00	0.54±0.00	3.53±0.19	0.23±0.00	0.45±0.01
KPG112a	0.452	3.80±0.47	0.35±0.00	0.59±0.00	3.55±0.45	0.30±0.00	0.47±0.00
KPG112b	...	4.13±0.20	0.43±0.00	0.58±0.01	3.60±0.46	0.30±0.00	0.42±0.01
KPG125a	1.724	3.39±0.31	0.18±0.00	0.22±0.00	3.40±0.29	0.17±0.00	0.19±0.00
KPG125b	...	2.66±0.15	0.40±0.00	0.44±0.01	2.75±0.15	0.36±0.00	0.36±0.00
KPG136a	1.190	2.96±0.37	0.24±0.01	0.29±0.00	3.02±0.38	0.20±0.00	0.16±0.00
KPG136b	...	3.58±0.36	0.25±0.01	0.25±0.00	3.51±0.35	0.19±0.00	0.12±0.00
KPG141a	2.836	3.51±0.16	0.40±0.01	0.85±0.01	3.64±0.17	0.39±0.00	0.87±0.01
KPG141b	...	2.90±0.30	0.44±0.00	0.26±0.00	2.94±0.31	0.45±0.00	0.29±0.00
KPG150a	2.273	4.41±0.30	0.10±0.00	0.12±0.00	4.25±0.28	0.15±0.00	0.13±0.00
KPG150b	...	3.38±0.14	0.19±0.00	0.26±0.00	3.52±0.15	0.19±0.00	0.20±0.00
KPG151a	0.641	4.50±0.17	0.51±0.01	1.05±0.01	4.30±0.23	0.37±0.01	0.85±0.01
KPG151b	...	4.03±0.29	0.36±0.01	0.35±0.01	3.90±0.27	0.33±0.02	0.25±0.01
KPG156a	0.889	3.06±0.12	0.33±0.01	0.41±0.00	3.20±0.13	0.29±0.00	0.31±0.00
KPG156b	...	3.47±0.30	0.20±0.00	0.23±0.00	3.44±0.30	0.18±0.00	0.28±0.00
KPG159a	1.278	2.77±0.48	0.12±0.00	0.31±0.22	2.92±0.52	0.11±0.00	0.37±0.23
KPG159b	...	3.10±0.31	0.12±0.00	0.20±0.12
KPG160a	0.963	3.45±0.23	0.06±0.00	0.18±0.00	3.38±0.22	0.06±0.00	0.14±0.00
KPG160b	...	3.21±0.27	0.31±0.01	0.86±0.02	3.27±0.28	0.37±0.01	0.80±0.01
KPG168a	0.718	3.76±0.33	0.07±0.00	0.16±0.00	3.66±0.31	0.06±0.00	0.15±0.00
KPG168b	...	3.76±0.31	0.20±0.01	0.54±0.02	3.64±0.25	0.17±0.02	0.11±0.01
KPG195a	0.680	3.67±0.41	0.20±0.00	0.22±0.00	3.61±0.40	0.16±0.00	0.23±0.00
KPG195b	...	3.62±0.25	0.33±0.00	0.70±0.02	3.53±0.25	0.27±0.01	0.39±0.02
KPG211a	0.907	3.75±0.22	0.10±0.00	0.17±0.00	3.79±0.22	0.09±0.00	0.11±0.00

TABLE 2—*Continued*

KPG	<i>R</i> -band			<i>I</i> -band			
	<i>SEP</i>	<i>C</i>	<i>A</i>	<i>S</i>	<i>C</i>	<i>A</i>	<i>S</i>
KPG211b	...	3.02±0.38	0.05±0.00	0.21±0.00	2.95±0.37	0.08±0.00	0.18±0.00
KPG216a	1.222	3.83±0.19	0.53±0.01	0.56±0.01	3.67±0.19	0.47±0.01	0.47±0.01
KPG216b	...	3.39±0.15	0.44±0.01	0.46±0.01	3.34±0.16	0.47±0.01	0.44±0.01
KPG249a	0.725	3.20±0.17	0.48±0.01	0.39±0.01	3.25±0.17	0.33±0.01	0.32±0.01
KPG249b	...	4.26±0.19	0.47±0.01	0.44±0.01	4.10±0.17	0.42±0.01	0.34±0.01
KPG295a	0.783	3.81±0.21	0.32±0.00	0.23±0.01	3.76±0.19	0.30±0.01	0.22±0.02
KPG295b	...	3.78±0.19	0.30±0.00	0.70±0.01	3.87±0.20	0.34±0.00	0.50±0.01
KPG302a	0.847	3.13±0.09	0.24±0.00	0.41±0.01	3.25±0.10	0.17±0.00	0.26±0.00
KPG302b	...	3.41±0.19	0.22±0.00	0.23±0.01	3.33±0.18	0.18±0.01	0.09±0.01
KPG313a	1.158	2.32±0.08	0.17±0.00	0.28±0.01	2.37±0.08	0.13±0.01	0.14±0.01
KPG313b	...	3.50±0.20	0.15±0.00	0.35±0.00	3.49±0.21	0.13±0.00	0.29±0.00
KPG332a	0.730	2.68±0.08	0.28±0.00	0.26±0.00	2.72±0.09	0.25±0.00	0.16±0.00
KPG332b	...	3.11±0.04	0.77±0.00	0.80±0.01	3.35±0.04	0.70±0.00	0.74±0.01
KPG347a	0.371	2.66±0.05	0.60±0.00	0.53±0.01	2.77±0.04	0.60±0.00	0.40±0.01
KPG347b	...	3.26±0.06	0.43±0.00	0.55±0.01	3.30±0.06	0.40±0.00	0.37±0.01
KPG389a	0.952	2.18±0.22	0.32±0.00	0.32±0.00	2.28±0.24	0.27±0.00	0.29±0.00
KPG389b	...	3.23±0.21	0.37±0.00	0.61±0.00	3.32±0.22	0.35±0.00	0.51±0.00
KPG396a	1.193	3.61±0.16	0.40±0.01	0.47±0.01	3.34±0.20	0.27±0.02	0.83±0.01
KPG396b	...	2.89±0.14	0.29±0.01	0.35±0.00	2.92±0.14	0.27±0.02	0.63±0.01
KPG404a	0.775	3.24±0.47	0.24±0.00	0.18±0.00	3.43±0.52	0.21±0.00	0.21±0.00
KPG404b	...	3.06±0.10	0.53±0.00	0.47±0.01
KPG426a	0.578	3.31±0.30	0.12±0.00	0.13±0.00	3.50±0.31	0.10±0.01	0.09±0.00
KPG426b	...	3.68±0.58	0.17±0.00	0.10±0.00	3.70±0.58	0.13±0.00	0.08±0.00
KPG440a	1.260	3.22±0.09	0.20±0.01	0.35±0.01	3.22±0.10	0.10±0.02	0.27±0.01
KPG440b	...	3.39±0.09	0.26±0.00	0.79±0.01
KPG455a	0.918	3.72±0.34	0.08±0.00	0.25±0.00	3.73±0.34	0.11±0.00	0.29±0.00
KPG455b	...	3.60±0.16	0.21±0.01	0.56±0.01	3.65±0.18	0.17±0.00	0.32±0.00

TABLE 3
AVERAGES AND 1σ VARIATIONS OF *CAS* PARAMETERS FOR (S+S) PAIRED GALAXIES.

	<i>B</i> -Band	<i>V</i> -Band	<i>R</i> -Band	<i>I</i> -Band
	All/SEP < 1	All/SEP < 1	All/SEP < 1	All/SEP < 1
<i>C</i>	3.21±0.53/3.31±0.52	3.32±0.51/3.40±0.45	3.33±0.45/3.40±0.42	3.35±0.42/3.41±0.40
<i>A</i>	0.28±0.16/0.28±0.16	0.27±0.15/0.27±0.16	0.26±0.15/0.27±0.16	0.23±0.12/0.22±0.11
<i>S</i>	0.35±0.25/0.31±0.28	0.37±0.22/0.36±0.21	0.33±0.17/0.32±0.16	0.28±0.15/0.27±0.12

TABLE 4
AVERAGES AND 1σ VARIATIONS OF *R*-BAND *CAS* PARAMETERS FOR (S+S) PAIRED, ISOLATED AND ULIR GALAXIES

	(S+S) All/SEP < 1/SEP > 1	Frei	ULIRGs/ULIRGs Advanced
<i>C</i>	3.33±0.45/3.40±0.42/3.25±0.49	3.32 ± 0.55	3.55 ± 0.74/3.57±0.80
<i>A</i>	0.26±0.15/0.27±0.16/0.25±0.13	0.12 ± 0.08	0.33 ± 0.17/0.27±0.13
<i>S</i>	0.33±0.17/0.32±0.16/0.34±0.20	0.23 ± 0.15	0.48 ± 0.40/0.42±0.40